

# Graph Kernels Based on Multi-scale Graph Embeddings

Wei Ye, Hao Tian, and Qijun Chen  
Tongji University, Shanghai 201804, China  
{yew, 2133036, qjchen}@tongji.edu.cn

**Abstract**—Graph kernels are conventional methods for computing graph similarities. However, most of the R-convolution graph kernels face two challenges: 1) They cannot compare graphs at multiple different scales, and 2) they do not consider the distributions of substructures when computing the kernel matrix. These two challenges limit their performances. To mitigate the two challenges, we propose a novel graph kernel called the Multi-scale Path-pattern Graph kernel (MPG), at the heart of which is the multi-scale path-pattern node feature map. Each element of the path-pattern node feature map is the number of occurrences of a path-pattern around a node. A path-pattern is constructed by the concatenation of all the node labels in a path of a truncated BFS tree rooted at each node. Since the path-pattern node feature map can only compare graphs at local scales, we incorporate into it the multiple different scales of the graph structure, which are captured by the truncated BFS trees of different depth. We use the Wasserstein distance to compute the similarity between the multi-scale path-pattern node feature maps of two graphs, considering the distributions of substructures. We empirically validate MPG on various benchmark graph datasets and demonstrate that it achieves state-of-the-art performance.

## I. INTRODUCTION

Graph-structured data is ubiquitous in many scenarios, such as protein-protein interaction networks, social networks, citation networks, and cyber-physical systems. One interesting and fundamental problem for graph-structured data is quantifying their similarities, which can be measured by graph kernels. Most of graph kernels belong to the family of the R-convolution kernels [1] that decompose graphs into substructures and compare them. There are many kinds of substructures used in graph kernels, such as walks [2]–[4] and paths [5], [6], subgraphs [7]–[10], and subtree patterns [11]–[16].

The R-convolution graph kernels have two main challenges. Firstly, when computing the similarity between two graphs, they count the number of occurrences of each unique substructure in each graph and aggregate the occurrences. The simple aggregation operation does not consider the distributions of substructures in each graph, which might restrict their ability to capture complex relationships between substructures. Secondly, many R-convolution graph kernels cannot compare graphs at multiple different scales. For example, WL [13], [14] computes the graph similarity at global scales, because subtrees only consider neighborhood structures of nodes; SP [5] computes the graph similarity at local scales, because shortest-paths do not take neighborhood structures into account. In many real world scenarios, graphs such as social networks have structures at multiple different scales. Figure 1 shows an

online discussion thread on Reddit<sup>1</sup>. Nodes represent users and edges represent that at least one of the connected two users responds to the other’s comment. We can see that this graph contains structures at multiple different scales, such as chain, ring, and star. Graph kernels should not only differentiate the overall shape of graphs, but also their small substructures.

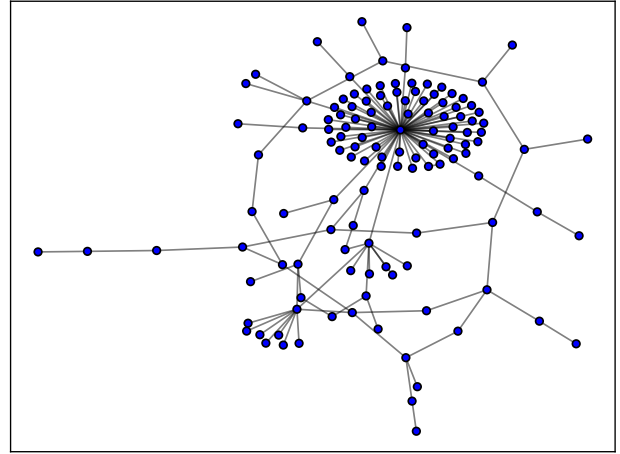


Fig. 1: A graph of a post on Reddit. Each node represents a user. Two users are connected by an edge if at least one of them responds to the other’s comment.

To solve the first challenge, PM [17] eigendecomposes the adjacency matrix of a graph and embeds each node in the space spanned by the eigenvectors. The similarity between two graphs is computed by the Earth Mover’s Distance [18] or the Pyramid Match kernel [19], [20], considering the distributions of node embeddings. However, eigenvectors can only capture the global connectivity of a graph. Thus, PM cannot compare graphs at multiple different scales. WWL [16] adopts the Weisfeiler-Lehman test of graph isomorphism [21] to relabel each node. The new label of a node corresponds to the subtree pattern around it. WWL considers node labels as categorical embeddings. The similarity between two graphs is computed by the Wasserstein distance, using the normalized Hamming distance as the ground distance for categorical node embeddings. The distributions of subtree patterns are considered in the computation of graph similarity. But WWL

<sup>1</sup><https://www.reddit.com/r/AskReddit>

cannot compare graphs at local scales because of the utilization of the subtree patterns as used in WL.

To solve the second challenge, MLG [10] computes graph similarity at multiple different scales by applying recursively the Feature space Laplacian Graph (FLG) kernel on a hierarchy of nested subgraphs. Specifically, FLG is a variant of the Bhattacharyya kernel [22] that computes the similarity between two graphs by using their Laplacian matrices. The sizes of subgraphs increase with the increasing level of the hierarchy, including the different scales of the graph structure around a node. However, MLG does not take the distributions of node embeddings (denoted by the rows of the graph Laplacian matrix) into account when computing graph similarity.

To mitigate the two challenges, in this paper, we propose a multi-scale path-pattern feature map<sup>2</sup> for each node in a graph, capturing the multi-scale graph structures around a node. The path-pattern node feature map is constructed by counting the number of occurrences of path-patterns around a node. Each path-pattern is denoted by the concatenation of the labels of all the nodes in a path from the root to any other node in the truncated BFS (Breadth-First Search) tree rooted at each node. To integrate the multi-scale graph structures into the path-pattern node feature map, we allow components in a path to be BFS trees of different depth and call such a path super path. To extract the path-pattern from super path, we project each BFS tree in a super path into an integer label by an injective hash function, i.e., hashing the same BFS trees to the same integer label and different BFS trees to different integer labels. We concatenate the multiple scales of path-pattern node feature maps and adopt the Wasserstein distance to compute graph similarity.

Our main contributions can be summarized as follows:

- We propose the path-pattern node feature map that is built on the paths in the truncated BFS tree rooted at each node and can compare graphs at local scales.
- We propose the multi-scale path-pattern node feature map that incorporates the different scales of the graph structure into the path-pattern node feature map and can compare graphs at multiple scales. The different scales of the graph structure are captured by the truncated BFS trees of varying depth rooted at each node.
- We develop a graph kernel called MPG (for Multi-scale Path-pattern Graph kernel) that employs the Wasserstein distance to compute the similarity between the multi-scale path-pattern node feature maps of two graphs.
- We show in the experiments that our method MPG achieves the best classification accuracy on most of the benchmark datasets.

The rest of the paper is organized as follows: We describe preliminaries in the following section. Section 3 introduces our approach, including path-pattern node feature map, multi-scale path-pattern node feature map, and our graph kernel MPG. Section 4 compares MPG with related techniques for graph

classification on the benchmark datasets. Section 5 discusses related work and Section 6 concludes the paper.

## II. PRELIMINARIES

### A. Notations

In this work, we use lower-case Roman letters (e.g.,  $a, b$ ) to denote scalars. We denote vectors (row) by boldface lower case letters (e.g.,  $\mathbf{x}$ ) and denote its  $i$ -th element by  $\mathbf{x}(i)$ . We use  $\mathbf{x} = [x_1, \dots, x_n]$  to denote creating a vector by stacking scalar  $x_i$  along the columns. We consider an undirected labeled graph  $\mathcal{G} = (\mathcal{V}, \mathcal{E}, l)$ , where  $\mathcal{V}$  is a set of nodes with number  $|\mathcal{V}|$  of nodes,  $\mathcal{E}$  is a set of graph edges with number  $|\mathcal{E}|$  of edges, and  $l : \mathcal{V} \rightarrow \Sigma$  is a function that assigns labels from a set of positive integers  $\Sigma$  to nodes. Without loss of generality,  $|\Sigma| \leq |\mathcal{V}|$ . An edge  $e$  is denoted by two nodes  $u, v$  that are connected to it. In graph theory [23], a walk is defined as a sequence of nodes, e.g., “ $v_1, v_2, \dots$ ” where consecutive nodes are connected by an edge. A trail is a walk that consists of all distinct edges. A path is a trail that consists of all distinct nodes and edges. The depth of a subtree is the maximum length of paths between the root and any other node in the subtree.

### B. Wasserstein Distance

The Wasserstein distance is a distance function defined between probability distributions on a given metric space  $M$ . Let  $\mu$  and  $\nu$  be two probability distributions on  $M$  and  $d$  be a ground distance such as the Euclidean distance. The  $p$ -th ( $p \geq 1$ ) Wasserstein distance between  $\mu$  and  $\nu$  is defined as follows:

$$W_p(\mu, \nu) := \left( \inf_{\gamma \in \Gamma(\mu, \nu)} \int_{M \times M} d(x, y)^p d\gamma(x, y) \right)^{1/p} \quad (1)$$

where  $\Gamma(\mu, \nu)$  denotes the collection of all probability distributions on  $M \times M$  with marginal distributions  $\mu$  and  $\nu$ , respectively.

The one-dimensional ( $p = 1$ ) Wasserstein distance is equivalent to the Earth Mover’s Distance [18]. Intuitively, if  $\mu$  and  $\nu$  are viewed as a unit amount of earth piled on  $M$ ,  $W_1(\mu, \nu)$  is the minimum cost of turning one pile into the other, which is assumed to be the amount of earth moved times the distance it has to be moved. In this paper, we compute the Wasserstein distance between two graphs (each graph is represented as a finite set of node embeddings). Thus, we use sum instead of integral in the computation of  $W_1(\mu, \nu)$ , which can be formulated and solved as an optimal transport problem [24]:

<sup>2</sup>In this work, feature map and embedding are used exchangeably.

$$\begin{aligned}
& \min \sum_{i=1}^{|\mathcal{V}|_1} \sum_{j=1}^{|\mathcal{V}|_2} f_{i,j} d(\mathbf{x}_i, \mathbf{y}_j) \\
& \text{subject to} \\
& \sum_{i=1}^{|\mathcal{V}|_1} f_{i,j} = \frac{1}{|\mathcal{V}|_2} \quad \forall j \in \{1, \dots, |\mathcal{V}|_2\} \\
& \sum_{j=1}^{|\mathcal{V}|_2} f_{i,j} = \frac{1}{|\mathcal{V}|_1} \quad \forall i \in \{1, \dots, |\mathcal{V}|_1\} \\
& f_{i,j} \geq 0 \quad \forall i \in \{1, \dots, |\mathcal{V}|_1\}, \forall j \in \{1, \dots, |\mathcal{V}|_2\}
\end{aligned} \tag{2}$$

where  $|\mathcal{V}|_1$  and  $|\mathcal{V}|_2$  stand for the number of nodes in graphs  $\mathcal{G}_1$  and  $\mathcal{G}_2$ , respectively.  $\mathbf{x}_i$  is the embedding vector of node  $v_i$  in graph  $\mathcal{G}_1$  and  $\mathbf{y}_j$  is the embedding vector of node  $u_j$  in graph  $\mathcal{G}_2$ .  $f_{i,j}$  is the  $(i, j)$ -th element of the flow matrix  $\mathbf{F} \in \mathbb{R}^{|\mathcal{V}|_1 \times |\mathcal{V}|_2}$ .  $d(\mathbf{x}_i, \mathbf{y}_j) = \|\mathbf{x}_i - \mathbf{y}_j\|_2$  denotes the Euclidean distance between two node embedding vectors.

After finding the optimal flow matrix  $\mathbf{F}$  that minimizes the above objective function,  $W_1(\mathbf{X}, \mathbf{Y})$  between the node embeddings of graphs  $\mathcal{G}_1$  and  $\mathcal{G}_2$  can be computed as follows:

$$W_1(\mathbf{X}, \mathbf{Y}) = \frac{\sum_{i=1}^{|\mathcal{V}|_1} \sum_{j=1}^{|\mathcal{V}|_2} f_{i,j} d(\mathbf{x}_i, \mathbf{y}_j)}{\sum_{i=1}^{|\mathcal{V}|_1} \sum_{j=1}^{|\mathcal{V}|_2} f_{i,j}} \tag{3}$$

### III. APPROACH

#### A. Path-Pattern Feature Map

We first define the path-pattern as follows:

**Definition 1** (Path-Pattern). *Given an undirected labeled graph  $\mathcal{G} = (\mathcal{V}, \mathcal{E}, l)$ , we build a truncated BFS tree  $\mathcal{T} = (\mathcal{V}', \mathcal{E}', l)$  ( $\mathcal{V}' \subseteq \mathcal{V}$  and  $\mathcal{E}' \subseteq \mathcal{E}$ ) of depth  $d$  rooted at each node  $v \in \mathcal{V}$ . The node  $v$  is called root. For each node  $v' \in \mathcal{V}'$ , there is a path  $P = "v, v_1, v_2, \dots, v'"$  from the root  $v$  to  $v'$  consisting of distinct nodes and edges. The concatenated labels  $l(P) = "l(v), l(v_1), l(v_2), \dots, l(v)"$  is called a path-pattern of  $\mathcal{G}$ .*

Note from this definition that a path-pattern could only contain the root node. Figure 2(a) and (b) show two example undirected labeled graphs  $\mathcal{G}_1$  and  $\mathcal{G}_2$ . Figure 2(c) and (d) show two truncated BFS trees of depth  $d = 1$  rooted at the nodes with label 4 in  $\mathcal{G}_1$  and  $\mathcal{G}_2$ , respectively. All the path-patterns of the root of the BFS tree in Figure 2(c) are "4", "4, 1", "4, 1", "4, 3" and those of the root of the BFS tree in Figure 2(d) are "4", "4, 1", "4, 3". For a set of graphs, we first build a truncated BFS tree of depth  $d$  rooted at each node and then generate all its path-patterns and store them in a multiset<sup>3</sup>  $\mathcal{M}$ .

We define the path-pattern graph feature map as follows:

**Definition 2** (Path-Pattern Graph Feature Map). *Let  $\mathcal{M}_1, \mathcal{M}_2, \dots, \mathcal{M}_n$  be the multisets of path-patterns corresponding to graphs  $\mathcal{G}_1, \mathcal{G}_2, \dots, \mathcal{G}_n$ . Let the union of*

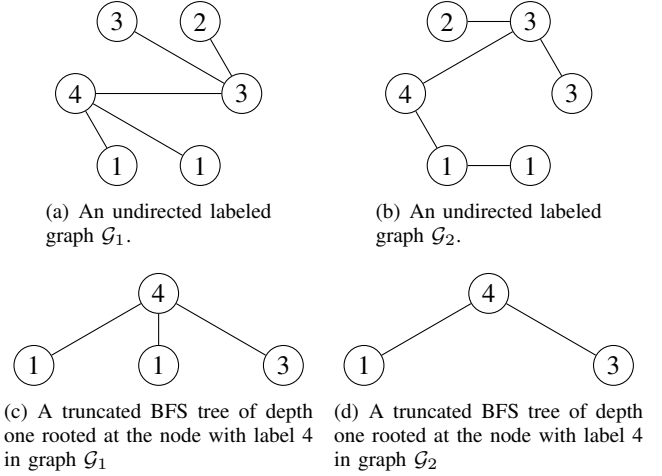


Fig. 2: Illustration of the path-patterns in graphs.  $\Sigma = \{1, 2, 3, 4\}$ .

all the multisets be a set  $\mathcal{U} = \mathcal{M}_1 \cup \mathcal{M}_2 \cup \dots \cup \mathcal{M}_n = \{l(P_1), l(P_2), \dots, l(P_{|\mathcal{U}|})\}$ . Define a map  $\psi : \{\mathcal{G}_1, \mathcal{G}_2, \dots, \mathcal{G}_n\} \times \Sigma \rightarrow \mathbb{N}$  such that  $\psi(\mathcal{G}_i, l(P_j))$  ( $1 \leq i \leq n, 1 \leq j \leq |\mathcal{U}|$ ) is the number of occurrences of the path-pattern  $l(P_j)$  in graph  $\mathcal{G}_i$ . Then, the path-pattern graph feature map of  $\mathcal{G}_i$  is defined as follows:

$$\phi(\mathcal{G}_i) = [\psi(\mathcal{G}_i, l(P_1)), \psi(\mathcal{G}_i, l(P_2)), \dots, \psi(\mathcal{G}_i, l(P_{|\mathcal{U}|}))] \tag{4}$$

#### B. Multi-scale Path-Pattern Feature Map

In the last section, we decompose a graph into its substructures, i.e., paths. However, paths cannot reveal the structural or topological information of nodes. Thus, the path-pattern feature map can only capture graph similarity at local scales. To capture graph similarity at multiple different scales, we focus on the different scales of the graph structure around a node.

To incorporate the multiple different scales of the graph structure into the path-pattern feature map, we extend the definition of path to super path as follows:

**Definition 3** (Super Path). *Given an undirected labeled graph  $\mathcal{G} = (\mathcal{V}, \mathcal{E}, l)$ , we build a truncated BFS tree  $\mathcal{T} = (\mathcal{V}', \mathcal{E}', l)$  ( $\mathcal{V}' \subseteq \mathcal{V}$  and  $\mathcal{E}' \subseteq \mathcal{E}$ ) of depth  $d$  rooted at each node  $v \in \mathcal{V}$ . The node  $v$  is called root. For each node  $v' \in \mathcal{V}'$ , there is a path  $P = "v, v_1, v_2, \dots, v'"$  from the root  $v$  to  $v'$  consisting of distinct nodes and edges. For each node in  $P$ , we build a truncated BFS tree of depth  $k$  rooted at it, which captures the graph structure at the  $k$ -th scale. The sequence of trees  $S = "\mathcal{T}_v, \mathcal{T}_{v_1}, \mathcal{T}_{v_2}, \dots, \mathcal{T}_{v}"$  is called a super path.*

We can see that the definition of super path includes that of path. Path is a special case of super path when the truncated BFS tree rooted at each distinct node in a path is of depth zero. Now we need to determine the path-pattern for a super path. The difficulty is how to label each truncated BFS tree in a super path. In this case, we also need to redefine the definition of the label function  $l$  described in Section II-A as

<sup>3</sup>A set that can contain the same element multiple times.

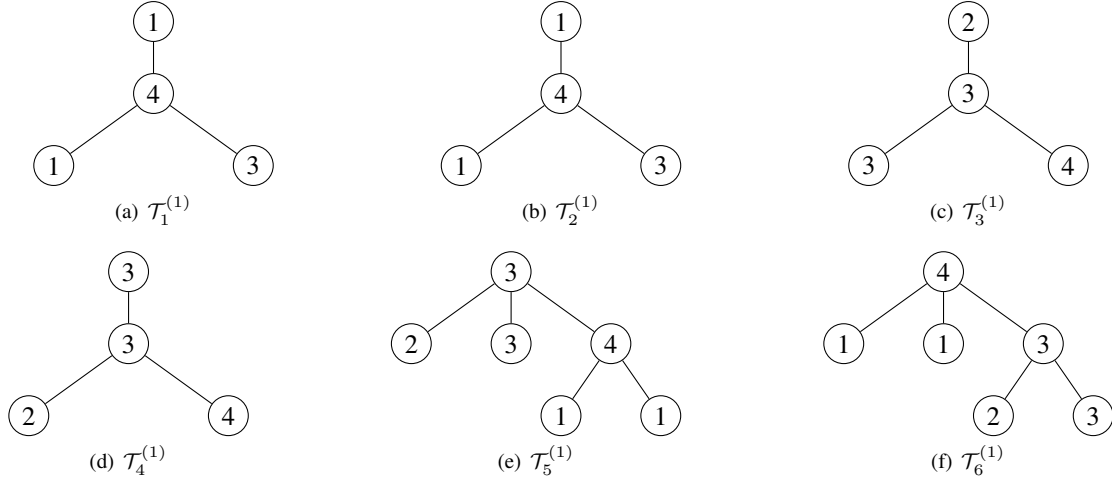


Fig. 3: A truncated BFS tree of depth one rooted at each node in the undirected labeled graph  $\mathcal{G}_1$ .

follows:  $l : \mathcal{T} \rightarrow \Sigma$  is a function that assigns labels from a set of positive integers  $\Sigma$  to trees. Thus, the definition of the path-pattern for super path is the concatenated labels  $l(S) = "l(\mathcal{T}_v), l(\mathcal{T}_{v_1}), l(\mathcal{T}_{v_2}), \dots, l(\mathcal{T}_{v'})"$ .

For each truncated BFS tree in a super path, we need to hash it to an integer label. The hash function should be injective, i.e., hashing the same two trees to the same integer label and different trees to different integer labels. In this paper, we use the concatenation of all the edges of a labeled BFS tree as a hash method. For example, in Figure 3,  $\mathcal{T}_1^{(1)}$  can be denoted by "1, 4, 4, 1, 4, 3", and  $\mathcal{T}_5^{(1)}$  can be denoted by "3, 2, 3, 3, 3, 4, 4, 1, 4, 1". Now, the label function  $l : \mathcal{T} \rightarrow \Sigma$  can assign the same positive integer label to the same trees (the same codeword).

In our implementation, we use a set to store BFS trees of depth  $k$  rooted at each node in a dataset of graphs. In this case, the set will only contain unique BFS trees. For BFS trees shown in Figure 3 and Figure 4, the set will contain  $\mathcal{T}_1^{(2)}$ ,  $\mathcal{T}_2^{(2)}$ ,  $\mathcal{T}_1^{(1)}/\mathcal{T}_2^{(1)}$ ,  $\mathcal{T}_3^{(1)}/\mathcal{T}_3^{(2)}$ ,  $\mathcal{T}_4^{(2)}$ ,  $\mathcal{T}_5^{(1)}$ ,  $\mathcal{T}_4^{(1)}/\mathcal{T}_5^{(2)}$ ,  $\mathcal{T}_6^{(1)}$ , and  $\mathcal{T}_6^{(2)}$ . Note that the truncated BFS trees in the set are sorted lexicographically. We can use the index of each truncated BFS tree in the set as its label. For instance,  $l : \mathcal{T}_1^{(2)} \rightarrow 1$ ,  $l : \mathcal{T}_2^{(2)} \rightarrow 2$ ,  $l : \mathcal{T}_1^{(1)}/\mathcal{T}_2^{(1)} \rightarrow 3$ ,  $l : \mathcal{T}_3^{(1)}/\mathcal{T}_3^{(2)} \rightarrow 4$ ,  $l : \mathcal{T}_4^{(2)} \rightarrow 5$ ,  $l : \mathcal{T}_5^{(1)} \rightarrow 6$ ,  $l : \mathcal{T}_4^{(1)}/\mathcal{T}_5^{(2)} \rightarrow 7$ ,  $l : \mathcal{T}_6^{(1)} \rightarrow 8$ , and  $l : \mathcal{T}_6^{(2)} \rightarrow 9$ . After considering the graph structure at the second scale around node 4 in  $\mathcal{G}_1$ , the super paths starting from node 4 are " $\mathcal{T}_6^{(1)}$ ", " $\mathcal{T}_6^{(1)}, \mathcal{T}_1^{(1)}$ ", " $\mathcal{T}_6^{(1)}, \mathcal{T}_2^{(1)}$ ", and " $\mathcal{T}_6^{(1)}, \mathcal{T}_5^{(1)}$ ". Their corresponding path-patterns are "8", "8, 3", "8, 3", and "8, 6", respectively.

**Theorem 1.** *The concatenation of all the edges in a labeled BFS tree is injective.*

*Proof.* If two labeled BFS trees each has only one edge, they are identical if and only if they have the same edge. So up to  $m = 1$  (edge number) the proof is true. Then, we follow an inductive reasoning and assume that if  $m = i$  the proof is

true, it is also true when  $m = i + 1$ .

In the case of  $m = i$ , for each of the two identical BFS trees, we need to attach a node to one of their leaf nodes. If and only if the edges that connect the leaf and attached nodes are identical, the two new BFS trees are identical. So up to  $m = i + 1$  the proof is also true. Thus, the concatenation of all the edges in a labeled BFS tree is injective, because it generates the same integer label for the same BFS trees and different integer labels for different BFS trees.  $\square$

Note that if the truncated BFS trees of the same depth rooted at two nodes are identical, the two nodes have the same scale of the graph structure around them. For example, Figure 3(a) and (b) show two truncated BFS trees rooted at the two nodes with the same label 1 in Figure 2(a). The two trees are identical, and thus these two nodes have the same second scale of the graph structure. This phenomenon also happens across graphs. For example, the nodes with label 2 in Figure 2(a) and (b) also have the same second scale of the graph structure. The corresponding BFS trees shown in Figure 3(c) and Figure 4(c) are identical. Figure 3(d) and (e) show another two truncated BFS trees rooted at the two nodes with the same label 3 in Figure 2(a). We can see that they have different second scale of the graph structure. Thus, by integrating the multiple different scales of the graph structure into path-patterns, we can distinguish path-patterns at multiple different scales. If we build truncated BFS trees of depth zero rooted at each node for super paths, the two path-patterns "1, 4, 3" in Figure 2(a) and "1, 4, 3" in Figure 2(b) (The starting node is the node with label 1 at the left-bottom corner.) are identical. However, if we build super paths using truncated BFS trees of depth two (as shown in Figure 3(a)(f)(e) and Figure 4(b)(f)(d), the two path-patterns become the two new path-patterns "3, 8, 6" and "2, 9, 5", which are totally different.

In this paper, we concatenate all the path-pattern graph feature maps at multiple different scales measured by the

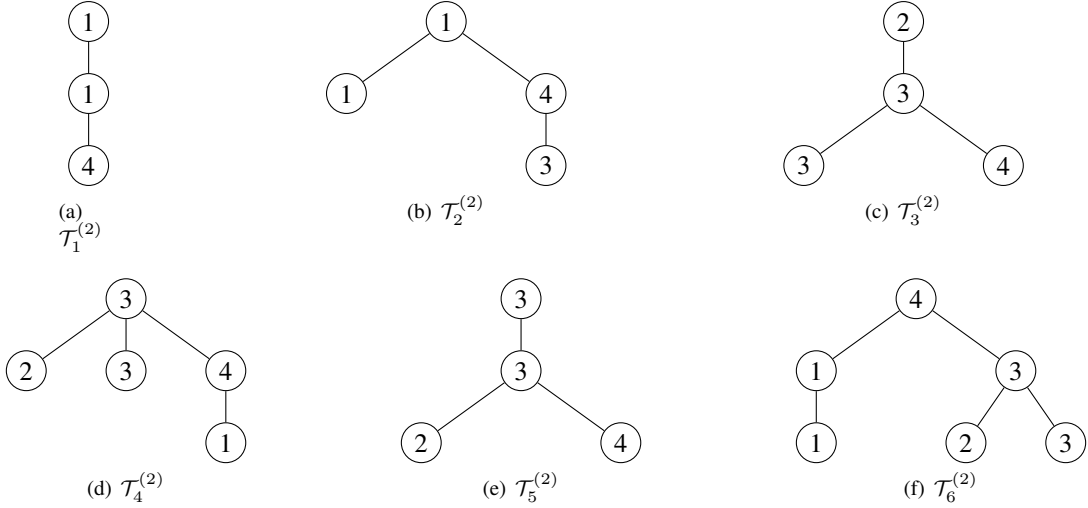


Fig. 4: A truncated BFS tree of depth one rooted at each node in the undirected labeled graph  $\mathcal{G}_2$ .

truncated BFS trees of depth  $k$  in the super path as follows:

$$\phi(\mathcal{G}) = \phi(\mathcal{G}^{(0)}) \parallel \phi(\mathcal{G}^{(1)}) \parallel \dots \parallel \phi(\mathcal{G}^{(k)}) \quad (5)$$

where  $\phi(\mathcal{G}^{(k)})$  corresponds to the path pattern graph feature map built on the super path with truncated BFS trees of depth  $k$  rooted at each node.

### C. Computing Graph Kernels

We define the path-pattern node feature map as follows:

**Definition 4** (Path-Pattern Node Feature Map). *For nodes in graph  $\mathcal{G}$ , define a map  $\psi : \{v_1, v_2, \dots, v_{|\mathcal{V}|}\} \times \Sigma \rightarrow \mathbb{N}$  where  $v_i \in \mathcal{V}$  ( $1 \leq i \leq |\mathcal{V}|$ ) such that  $\psi(v_i, l(P_j))$  ( $1 \leq i \leq |\mathcal{V}|, 1 \leq j \leq |\mathcal{U}|$ ) is the number of occurrences of the path-pattern  $l(P_j)$  that starts from  $v_i$  in graph  $\mathcal{G}$ . Then, the path-pattern node feature map of  $v_i$  is defined as follows:*

$$\phi(v_i) = [\psi(v_i, l(P_1)), \psi(v_i, l(P_2)), \dots, \psi(v_i, l(P_{|\mathcal{U}|}))] \quad (6)$$

Similar to Equation (5), we get the multi-scale path-pattern node feature map as follows:

$$\phi(v_i) = \phi(v_i^{(0)}) \parallel \phi(v_i^{(1)}) \parallel \dots \parallel \phi(v_i^{(k)}) \quad (7)$$

where  $\phi(v_i^{(k)})$  is the path-pattern node feature map built on  $\mathcal{G}^{(k)}$ .

The multi-scale path-pattern node feature maps will be used as node embeddings. We can see that the multi-scale path-pattern graph feature map equals to the sum of all the multi-scale path-pattern node feature maps in that graph, i.e.,

$$\phi(\mathcal{G}) = \sum_{i=1}^{|\mathcal{V}|} \phi(v_i) \quad (8)$$

In this paper, we first use Equation (3) to compute the distance between the multi-scale path-pattern node feature maps of two graphs  $\mathcal{G}_1$  and  $\mathcal{G}_2$  and then use the Laplacian RBF kernel to construct our graph kernel MPG:

$$\mathbf{K}(\mathcal{G}_1, \mathcal{G}_2) = \exp(-\lambda W_1(\mathbf{X}, \mathbf{Y})) \quad (9)$$

where  $\lambda$  is a hyperparameter and the  $i$ -th row of  $\mathbf{X}$  or  $\mathbf{Y}$  contains the multi-scale path-pattern node feature map  $\phi(v_i)$ .

Note that the Wasserstein distance, despite being a metric, in its general form is not isometric (i.e., no metric-preserving mapping to the  $l_2$  norm) as argued in [16], owing to that the metric space induced by it strongly depends on the chosen ground distance [25]. Thus, we cannot derive a positive semi-definite kernel from the Wasserstein distance in its general form, because the conventional methods [26] cannot be applied on it. Thus, MPG is not a positive semi-definite kernel. However, we can still employ Kreĭn SVM (KSVM) [27] for learning with indefinite kernels. Generally speaking, kernels that are not positive semi-definite induce reproducing kernel Kreĭn spaces (RKKS), which is a generalization of reproducing kernel Hilbert spaces (RKHS). KSVM can solve learning problems in RKKS.

### D. Computational Complexity Analysis

In this section, we provide the pseudo-code of our MPG graph kernel in Algorithm 1. Line 2 in Algorithm 1 uses Algorithm 2 to generate all the paths in a set of graphs  $\mathcal{G}$ . For each node  $v$  in graph  $\mathcal{G}_i$  (lines 4–9 in Algorithm 2), we build a truncated BFS tree of depth  $d$  rooted at it. The time complexity of BFS traversal of a graph is  $\mathcal{O}(|\mathcal{V}| + |\mathcal{E}|)$ , where  $|\mathcal{V}|$  is the number of nodes, and  $|\mathcal{E}|$  is the number of edges in a graph. For convenience, we assume that  $|\mathcal{E}| > |\mathcal{V}|$  and all the  $n$  graphs have the same number of nodes and edges. Thus, the worst time complexity of Algorithm 2 for all the  $n$  graphs is  $\mathcal{O}(n \cdot |\mathcal{V}| \cdot (|\mathcal{E}| + |\mathcal{V}|))$ .

Line 3 in Algorithm 1 uses Algorithm 3 to relabel each node (i.e., hashing each truncated BFS tree of depth  $k$  to an integer label, capturing the multiple different scales of the graph structure) for the preparation of constructing the super paths. Like Algorithm 2, for each node in each graph, Algorithm 3 also constructs a BFS tree of depth  $k$ . The worst time complexity of Algorithm 3 is  $\mathcal{O}(k \cdot n \cdot |\mathcal{V}| \cdot (|\mathcal{E}| + |\mathcal{V}|))$ .

Lines 6–10 in Algorithm 1 generate all the path-patterns corresponding to the same value of  $k$  (i.e., the same scale of the graph structure). The number of paths generated by Algorithm 2 is at most  $n \cdot |\mathcal{V}|^2$ . The time complexity of lines 6–10 in Algorithm 1 is  $\mathcal{O}(n \cdot |\mathcal{V}|^2 \cdot |\mathcal{E}|)$ .

Line 11 in Algorithm 1 sorts the elements in  $\mathcal{U}^{(i)}$  lexicographically, of which the time complexity is bounded by  $\mathcal{O}(|\mathcal{E}|)$  [14]. Lines 12–15 in Algorithm 1 count the number of occurrences of each unique path-pattern in  $\mathcal{U}^{(i)}$  around each node. The counting time complexity for a node is bounded by  $\mathcal{O}(q \cdot |\mathcal{V}|)$ , where  $q$  is the maximum length of all  $\mathcal{U}^{(i)}$  ( $0 \leq i \leq k$ ). Thus, the time complexity of lines 12–15 in Algorithm 1 is  $\mathcal{O}(n \cdot |\mathcal{V}| \cdot q \cdot |\mathcal{V}|)$ . The time complexity of lines 4–15 in Algorithm 1 is  $\mathcal{O}(k \cdot n \cdot |\mathcal{V}|^2 \cdot (q + |\mathcal{E}|))$ . Since  $|\mathcal{E}| \gg q$ , the time complexity of lines 4–15 in Algorithm 1 is bounded by  $\mathcal{O}(k \cdot n \cdot |\mathcal{V}|^2 \cdot |\mathcal{E}|)$ .

Lines 18–19 in Algorithm 1 first compute the Wasserstein distance between the two embeddings of graphs  $\mathcal{G}_i$  and  $\mathcal{G}_j$  and then compute the Laplacian RBF kernel. The time complexity of computing the Wasserstein distance is  $\mathcal{O}(|\mathcal{V}|^3 \cdot \log(|\mathcal{V}|))$  [28]. For  $n$  graphs, the time complexity to compute the kernel matrix is  $\mathcal{O}(n^2 \cdot |\mathcal{V}|^3 \cdot \log(|\mathcal{V}|))$ . The total time complexity of our MPG graph kernel is bounded by  $\mathcal{O}(k \cdot n \cdot |\mathcal{V}|^2 \cdot |\mathcal{E}| + n^2 \cdot |\mathcal{V}|^3 \cdot \log(|\mathcal{V}|))$ .

---

#### Algorithm 1: MPG

---

**Input:** A set of graphs  $\mathcal{G} = \{\mathcal{G}_1, \mathcal{G}_2, \dots, \mathcal{G}_n\}$  and the initial label function  $l : \mathcal{V} \rightarrow \Sigma$ ,  $d, k, \lambda$

**Output:** The computed kernel matrix  $\mathbf{K} \in \mathbb{R}^{n \times n}$

```

1  $\mathbf{K} \leftarrow \text{zeros}((n, n));$ 
2 all_graph_paths  $\leftarrow$  Path_Generation ( $\mathcal{G}, d$ );
3 all_labels  $\leftarrow$  Graph_Relabeling ( $\mathcal{G}, l, k$ );
4 for  $i \leftarrow 0$  to  $k$  do
5    $\mathcal{U}^{(i)} \leftarrow \text{set}(\ )$ ,  $l^{(i)} \leftarrow \text{all\_labels}[i]$ ;
6   for  $j \leftarrow 1$  to  $n$  do
7     graph_path  $\leftarrow$  all_graph_paths[ $j$ ];
8     foreach node_path  $\in$  graph_path do
9       foreach path  $P$  in node_path do
10         $\mathcal{U}^{(i)}$ .add( $l^{(i)}(P)$ );
11    $\mathcal{U}^{(i)} \leftarrow \text{sort}(\mathcal{U}^{(i)})$ ; /* lexicographically */
12   for  $j \leftarrow 1$  to  $n$  do
13     foreach node  $v \in \mathcal{G}_j$  do
14        $\phi(v) \leftarrow [\psi(v, l^{(i)}(P_1)), \psi(v, l^{(i)}(P_2)), \dots$ 
15          $\dots, \psi(v, l^{(i)}(P_{|\mathcal{U}^{(i)}|}))]$ ;
16        $\Phi_j^{(i)} \leftarrow [\phi(v_1); \phi(v_2); \dots; \phi(v_{|\mathcal{V}_j|})]$ ;
17   for  $j \leftarrow 1$  to  $n$  do
18      $\Phi_j \leftarrow [\Phi_j^{(0)} \parallel \Phi_j^{(1)} \parallel \dots \parallel \Phi_j^{(k)}]$ ;
19   foreach pair of graphs  $\mathcal{G}_i$  and  $\mathcal{G}_j$  do
20      $\mathbf{K}(\mathcal{G}_i, \mathcal{G}_j) \leftarrow \exp(-\lambda W_1(\Phi_i, \Phi_j))$ ;
21 return  $\mathbf{K}$ ;

```

---



---

#### Algorithm 2: Path Generation

---

**Input:** A set of graphs  $\{\mathcal{G}_1, \mathcal{G}_2, \dots, \mathcal{G}_n\}$  and the depth  $d$  of the BFS tree rooted at each node

**Output:** All the paths in these graphs

```

1 all_graph_paths  $\leftarrow$  [];
2 for  $i \leftarrow 1$  to  $n$  do
3   graph_paths  $\leftarrow$  [];
4   foreach node  $v \in \mathcal{G}_i$  do
5     node_paths  $\leftarrow$  [];
6     Build a truncated BFS tree  $\mathcal{T}$  of depth  $d$  rooted
7     at node  $v$ ;
8     foreach node  $v' \in \mathcal{T}$  do
9       node_paths.append( $P$ );
10      /*  $P = "v, v_1, v_2, \dots, v'"$  */
11     graph_paths.append(node_paths);
12 all_graph_paths.append(graph_paths);
13 return all_graph_paths;

```

---



---

#### Algorithm 3: Graph Relabeling

---

**Input:** A set of graphs  $\mathcal{G} = \{\mathcal{G}_1, \mathcal{G}_2, \dots, \mathcal{G}_n\}$  and the initial label function  $l : \mathcal{T} \rightarrow \Sigma$ , the depth  $k$  of the BFS tree rooted at each node for capturing the multiple different scales of the graph structure

**Output:** The labels of each BFS tree

```

1 all_labels  $\leftarrow$  [];
2 for  $i \leftarrow 0$  to  $k$  do
3    $l^{(i)} \leftarrow$  [];
4   for  $j \leftarrow 1$  to  $n$  do
5     label  $\leftarrow$  [];
6     foreach node  $v \in \mathcal{G}_j$  do
7       Build a truncated BFS tree  $\mathcal{T}_v$  of depth  $i$ 
8       rooted at node  $v$ ;
9       label.append( $l(\mathcal{T}_v)$ );
10     $l^{(i)}$ .append(label)
11 all_labels.append( $l^{(i)}$ );
12 return all_labels;

```

---

## IV. EXPERIMENTAL EVALUATION

### A. Experimental Setup

We run all the experiments on a server with a dual-core Intel(R) Xeon(R) Gold 6226R CPU @ 2.90GHz, 256 GB memory, and Ubuntu 18.04.6 LTS operating system. MPG is written in Python. We make our code publicly available at Github<sup>4</sup>.

We compare MPG with nine state-of-the-art graph kernels. A brief description for each comparison graph kernel method is given as follows:

<sup>4</sup><https://github.com/yeweiysz/MPG>

- 1) **MLG** [10] is called the Multiscale Laplacian Graph kernel that builds a hierarchy of nested subgraphs to capture the graph structures at multiple different scales.
- 2) **RetGK** [4] introduces the return probabilities features (RPF) generated by random walks as a structural role descriptor for nodes. The RPF of each node is then embedded into the Hilbert space where the corresponding graph kernels are derived by the Maximum Mean Discrepancy (MMD) [29].
- 3) **PK** [30] is a propagation kernel, which is based on measuring how information spreads through the graph structure. It leverages early-stage distributions of random walks to capture structural information hidden in node neighborhood.
- 4) **PM** [17] embeds nodes into vectors by eigendecomposing the graph adjacency matrix and uses the Pyramid Match kernel [19], [20] to compute the similarity between the node embeddings of two graphs.
- 5) **WL** [14] is based on the Weisfeiler-Lehman test of graph isomorphism [31] for graphs. It counts the number of occurrences of each subtree pattern in graphs.
- 6) **Tree++** [6] counts the number of occurrences of path-patterns in graphs. It belongs to the R-convolution kernels without considering the distributions of the individual substructures in graphs.
- 7) **DGK** [32] considers graph substructures in graphs as words in documents and uses word2vec [33] to learn latent representations for graph substructures used in graph kernels such as GK [7], SP [5], and WL [14]. The similarity matrix between graph substructures is computed and integrated into the graph kernel matrix.
- 8) **WWL** [16] is an extension of WL. It also adopts the Wasserstein distance to compute the similarity between the node embeddings of two graphs.
- 9) **GNTK** [34] fuses graph neural networks with graph kernels. It is inspired by the recent connections between over-parameterized neural networks and kernel methods, i.e., neural tangent kernel [35]. It corresponds to infinitely wide multi-layer GNNs trained by gradient descent.

We also compare the multi-scale graph embedding method in MPG with other graph embedding methods. Specifically, we use other graph embedding methods to generate node embeddings and apply the Wasserstein distance to compute the corresponding graph kernels. A brief description for each graph embedding method is given as follows:

- 1) **DeepWalk** [36] performs the truncated random walks on graphs and considers each node sequence generated by the truncated random walk as a “natural language sentence”. The Skip-gram [33], [37] model is used to learn the word (node) embeddings in the “natural language sentence”.
- 2) **node2vec** [38] is an extension to DeepWalk by designing a biased random walk procedure. The biased random walk uses two sampling strategies, i.e., breath-first sampling and depth-first sampling, to search for the neighborhood more diversely.

- 3) **LINE** [39] optimizes an objective that preserves the first- and second-order graph structures in the embedding space. The first-order graph structure means the direct links between nodes while the second-order graph structure means the latent proximity between nodes that have the shared neighborhoods.
- 4) **GraRep** [40] proposes to preserve different  $k$ -step relational information in a graph in different subspaces, capturing multi-scale graph structural information. Each  $k$ -step relational information is represented by the  $k$ -th order of the positive log probability matrix, which is factorized by SVD for graph embedding.
- 5) **NetMF** [41] analyzes several Skip-gram-model-based graph embedding methods and unifies them in the framework of matrix factorization. It proposes to factorize the closed-form of DeepWalk’s implicit matrix by SVD.
- 6) **struc2vec** [42] learns node embeddings considering their structural identities in the graph. Nodes that have similar structural identities have close embeddings. The structural similarities between different nodes are encoded in a multilayer graph, which is also used to generate structural context for nodes.

We set the parameters for our MPG graph kernel as follows: The depth  $d$  of the truncated BFS tree rooted at each node for constructing the path-patterns is chosen from  $\{0, 1, 2, \dots, 6\}$ , and the depth  $k$  of the truncated BFS tree for constructing the super path (capturing the graph structure at multiple different scales) is chosen from  $\{0, 1, 2, \dots, 6\}$  as well. The parameters of the comparison methods are set according to their original papers. We use the implementations of MLG, PK, PM, and WL from the GraKeL [43] library. The implementations of other methods are obtained from their official websites.

We use 10-fold cross-validation with a binary  $C$ -SVM [44] (or a KSVM [27] in the case of MPG and WWL) to test classification accuracy of each method. The parameter  $C$  for each fold is independently tuned from  $\{10^{-3}, 10^{-2}, \dots, 10^3\}$  using the training data from that fold. We also tune the parameter  $\lambda$  from  $\{10^{-4}, 10^{-3}, \dots, 10^1\}$  for MPG and other graph-embedding-based graph kernels. We repeat the experiments ten times and report the average classification accuracy and standard deviation.

## B. Datasets

In order to test the performance of our graph kernel MPG, we adopt 15 benchmark datasets whose statistics are given in Table I. All the datasets are downloaded from Kersting et al. [45]. A short description for each dataset is given as follows:

- **Brain network dataset.** KKI [46] is a brain network constructed for the task of Attention Deficit Hyperactivity Disorder (ADHD) classification. Each node represents a region of interest (ROI) from the whole brain functional resonance image (fMRI) atlas, and each edge represents the correlation relationship between two ROIs.
- **Chemical compound datasets.** The MUTAG [47] dataset consists of 188 chemical compounds, which can be divided

TABLE I: Statistics of the benchmark datasets used in the experiments. Mean SP length stands for the average length of all the shortest-paths in a graph while Max SP length stands for the maximal length of all the shortest-paths in a graph.

Dataset	Size	Class #	Average node #	Average edge #	Node label #	Mean SP length	Max SP length
KKI	83	2	26.96	48.42	190	4.68	19
MUTAG	188	2	17.93	19.79	7	3.87	15
BZR_MD	306	2	21.30	225.06	8	1.00	1
DHFR_MD	393	2	23.87	283.01	7	1.00	1
NCI1	4110	2	29.87	32.30	37	7.27	45
NCI109	4127	2	29.68	32.13	38	7.19	61
PTC_MM	336	2	13.97	14.32	20	5.34	30
PTC_MR	344	2	14.29	14.69	18	5.70	30
PTC_FM	349	2	14.11	14.48	18	5.23	30
PTC_FR	351	2	14.56	15.00	19	5.54	30
ENZYMES	600	6	32.63	62.14	3	5.72	37
PROTEINS	1113	2	39.06	72.82	3	10.55	64
DD	1178	2	284.32	715.66	82	16.84	83
FIRSTMM_DB	41	11	1377.27	3074.10	5	26.44	94
Cuneiform	267	30	21.27	44.80	3	2.30	3

into two classes according to their mutagenic effect on a bacterium. The datasets BZR\_MD, DHFR\_MD are from [48]. These chemical compounds are represented by graphs, of which edges represent the chemical bond types (single, double, triple or aromatic), nodes represent atoms and node labels indicate atom types. BZR is a dataset of ligands for the benzodiazepine receptor. DHFR has 756 inhibitors of dihydrofolate reductase. BZR\_MD and DHFR\_MD are derived from BZR and DHFR, respectively, by removing explicit hydrogen atoms. The chemical compounds in the datasets BZR\_MD and DHFR\_MD are complete graphs. NCI1 and NCI109 [49] are two balanced subsets of dataset of chemical compounds screened for activity against non-small cell lung cancer and ovarian cancer cell lines, respectively.

- **Molecular compound datasets.** The PTC [50] dataset consists of compounds labeled according to carcinogenicity on rodents divided into male mice (MM), male rats (MR), female mice (FM) and female rats (FR). ENZYMES is a dataset of protein tertiary structures from [51], consisting of 600 enzymes from six Enzyme Commission top-level enzyme classes. The dataset PROTEINS [51] consists of proteins represented by graphs, whose nodes represent the secondary structure elements and edges represent that two nodes are neighbors along the amino acid sequence or three-nearest neighbors to each other in space. DD [52] is a dataset of protein structures represented by graphs. Nodes represent amino acids and two nodes are connected by an edge if they are less than six Ångstroms apart.
- **Point cloud dataset.** FIRSTMM\_DB [53] is a point cloud dataset, which contains 41 simulated 3D point clouds of household objects. Each object is represented by a  $k$ -nearest neighbor graph with respect to the Euclidean distance of the points in 3D space. Each node represents a point. If two points are  $k$ -nearest neighbors, they are connected by an edge. Each node has a label that represents the semantic parts, i.e., top, middle, bottom, handle, and usable-area, of the objects. The objects in FIRSTMM\_DB can be divided into 11 classes, i.e., cup, glass, can, knife, pot, pan, bowl,

kitchen tool, screw-driver, hammer, and bottle. Figure 5 shows the 3D point clouds of three example objects.

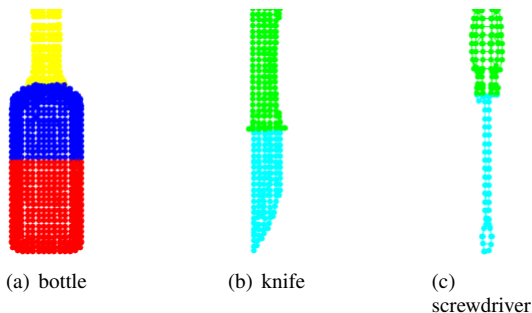


Fig. 5: Point clouds of household objects represented by semantic 4-nn graphs with semantic part labels top (yellow), middle (blue), bottom (red), usable-area (cyan), and handle (green). The edges are colored by the mean color of its connected nodes.

- **Cuneiform dataset.** The Cuneiform dataset [54] contains graphs representing 30 different Hittite cuneiform signs, each of which consists of tetrahedron shaped markings called wedges. The visual appearance of wedges can be classified according to the stylus orientation into vertical, horizontal, and diagonal. Each type of wedge is represented by a graph consisting of four vertices (nodes), i.e., right vertex, left vertex, tail vertex, and depth vertex. Thus, each node has two kinds of labels, one denoting the type of wedge it belongs to and the other denoting a point (depth, tail, right, left) of the wedge. Figure 6 shows the Cuneiform tablet and the graph representation of sign 2.

### C. Results

1) *Classification Accuracy:* Table II demonstrates the comparison of classification accuracy of MPG to other graph kernels on the benchmark datasets. We can see that MPG achieves the best classification accuracy on 10 datasets. On ENZYMES dataset, MPG has a gain of 10.4% over the best comparison method RetGK and a gain of 136.5% over the

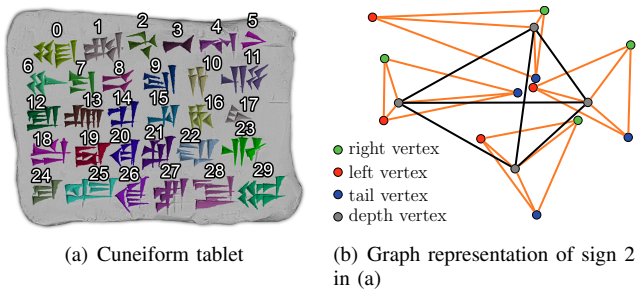


Fig. 6: Each wedge in each sign has four points that are represented by the four vertices (depth, tail, right, left) in a graph (as shown in (b)). The stylus orientations of wedges have three types, i.e., vertical, horizontal, and diagonal. (This figure is adopted from [54].)

worst comparison method PM. MPG is outperformed by other methods on the five datasets, i.e., KKI, MUTAG, PTC\_MR, DD, and Cuneiform. On datasets KKI and Cuneiform, Tree++ achieves the best results. On datasets MUTAG and DD, RetGK achieves the best classification accuracy, but the performance of MPG is on par with that of RetGK. On dataset PTC\_MR, WWL achieves the best result.

Graph kernels PK, WL, and Tree++ are the instances of the R-convolution kernels, which do not consider the distributions of the individual substructures in graphs and underperform on most of the datasets. MLG is a multi-scale graph kernel that computes graph similarities at multiple different scales. It does not take into account the distributions of individual substructures in graphs as well. Like our method MPG, all the three comparison methods RetGK, PM, and WWL embed each graph into the vector space and consider each graph as a set of node embeddings. The similarity between two graphs are derived by computing the similarity between their node embeddings using Maximum Mean Discrepancy [29] (adopted by RetGK), the Pyramid Match kernel (adopted by PM), and the Wasserstein distance (adopted by WWL). MPG outperforms all of them on most of the datasets, which proves that the multi-scale path-pattern node feature map used in MPG captures more information than the return probability features used in RetGK, the eigenvectors of the graph adjacency matrix used in PM, and the subtree feature map used in WWL. DGK and GNTK are two deep graph kernels, which integrate deep neural networks into the computation of kernel matrix. However, MPG also outperforms both of them on most of the datasets.

Since at the heart of MPG is the multi-scale path-pattern node feature maps (embeddings), we also compare the classification accuracy of MPG to other graph-embedding-based graph kernels. Each graph has two modalities, i.e., the graph structure and node labels. For the graph structure, we use graph embedding methods to generate the node embeddings. For node labels, we use one-hot encodings to represent them. We use the same method as used in MPG to compute the graph kernel matrix for each modality. The two types of

graph kernel matrices are combined by the Hadamard product. The results are shown in Table III. We can see that MPG significantly outperforms all the graph embedding methods on 13 datasets. Specifically, MPG’s performance on dataset FIRSTMM\_DB is about two times those of graph embedding methods. NetMF achieves the best result on dataset BZR\_MD. struc2vec achieves the best result on dataset Cuneiform, whose nodes have four different structural roles as demonstrated in Figure 6(b). It is beneficial to embed nodes with the same structural role into the same embedding.

2) *Parameter Sensitivity*: To analyze parameter sensitivity with regard to the two parameters  $d$  and  $k$  of MPG, we compute average classification accuracy over the 10-fold for all the combinations of  $d$  and  $k$ , where  $d, k \in \{0, 1, 2, \dots, 6\}$ , on datasets KKI, MUTAG, DHFR\_MD, and PTC\_FM. Figure 7 shows the heatmaps of the results. We can see that on each dataset the best result is achieved in a range with boundary values being less than or equal to the average length of all the shortest-paths of that dataset. For example, the average length of all the shortest-paths of dataset MUTAG is 3.87 (see Table I) and the best result is achieved when  $k = 0$  and  $d = 1$ ; the average length of all the shortest-paths of dataset PTC\_FM is 5.23 and the best result is achieved when  $k = 5$  and  $d = 0$ . This finding prevents us from searching for a large range of parameters in order to find the best result. On datasets KKI and DHFR\_MD, the classification accuracy remains stable when the values of  $k$  and  $d$  exceed a threshold. To explain this phenomenon, we check the multi-scale path-pattern feature map of each node in dataset DHFR\_MD and find that its dimension does not change when varying  $d$  with  $k$  fixed. This happens because the multi-scale path-pattern node feature map of dataset DHFR\_MD is at its full capacity.

3) *Running Time*: In this section, we report the running time needed to compute the kernel matrix of MPG on datasets KKI, MUTAG, DHFR\_MD, and PTC\_FM. We vary the number of depth  $d$  and  $k$ . The running time is demonstrated in Figure 8. For the case of varying the number of  $d$ , we fix  $k$  to the value of one; for the case of varying the number of  $k$ , we fix  $d$  to the value of one. We can see from Figure 8(a) that the running time of MPG on dataset DHFR\_MD remains stable, because the dimension of the path-pattern node feature map does not change when increasing the number of  $d$ . On datasets KKI and MUTAG, the running time of MPG increases linearly with respect to the depth  $d$ ; on dataset PTC\_FM, the running time of MPG increases quadratically with respect to the depth  $d$ . Figure 8(b) shows the running time versus the depth  $k$ . Note that y-axis is in the log scale. The running time of MPG on all the four datasets increases approximately linearly with respect to the depth  $k$ .

## V. RELATED WORK

In this section, we discuss the related literature to our work in two categories: graph kernels and graph embeddings.

### A. Graph Kernels

Random walk graph kernels [2], [3] first extract random walks from two graphs and then count the number of matching

TABLE II: Comparison of classification accuracy (mean  $\pm$  standard deviation) of MPG to other graph kernels on the benchmark datasets. N/A means the results are not reproducible because the current codes of GraKeL do not support that specific dataset.  $\dagger$  means the results are adopted from the original papers.

Dataset	MPG	MLG	RetGK	PK	PM	WL	Tree++	DGK	WWL	GNTK
KKI	55.4 $\pm$ 5.2	48.0 $\pm$ 3.6	48.5 $\pm$ 3.0	50.9 $\pm$ 4.2	52.3 $\pm$ 2.5	50.4 $\pm$ 2.8	<b>55.6<math>\pm</math>1.7<math>\dagger</math></b>	51.3 $\pm$ 4.2	45.4 $\pm$ 12.7	48.5 $\pm$ 2.9
MUTAG	89.9 $\pm$ 5.0	84.2 $\pm$ 2.6 $\dagger$	<b>90.3<math>\pm</math>1.1<math>\dagger</math></b>	84.5 $\pm$ 0.6 $\dagger$	85.6 $\pm$ 0.6 $\dagger$	82.1 $\pm$ 0.4 $\dagger$	87.4 $\pm$ 1.1	87.4 $\pm$ 2.7 $\dagger$	87.3 $\pm$ 1.5 $\dagger$	90.0 $\pm$ 8.5 $\dagger$
BZR_MD	<b>70.6<math>\pm</math>5.3</b>	48.9 $\pm$ 2.4	62.8 $\pm$ 1.7	61.5 $\pm$ 1.3	68.2 $\pm$ 1.2	59.7 $\pm$ 1.5	69.5 $\pm$ 1.1 $\dagger$	58.5 $\pm$ 1.5	69.9 $\pm$ 7.8	66.6 $\pm$ 2.3
DHFR_MD	<b>73.5<math>\pm</math>5.2</b>	67.9 $\pm$ 0.1	64.4 $\pm$ 1.0	64.2 $\pm$ 1.0	66.2 $\pm$ 1.0	64.0 $\pm$ 0.5	68.9 $\pm$ 0.9 $\dagger$	67.9 $\pm$ 0.3	67.9 $\pm$ 1.1	64.9 $\pm$ 1.5
NCI1	<b>86.5<math>\pm</math>0.9</b>	80.8 $\pm$ 1.3 $\dagger$	84.5 $\pm$ 0.2 $\dagger$	84.5 $\pm$ 0.1 $\dagger$	69.7 $\pm$ 0.1 $\dagger$	82.2 $\pm$ 0.2 $\dagger$	85.8 $\pm$ 0.1 $\dagger$	80.3 $\pm$ 0.5 $\dagger$	85.8 $\pm$ 0.3 $\dagger$	84.2 $\pm$ 1.5 $\dagger$
NCI109	<b>86.7<math>\pm</math>1.6</b>	81.3 $\pm$ 0.8 $\dagger$	80.1 $\pm$ 0.5	83.5 $\pm$ 0.1 $\dagger$	68.4 $\pm$ 0.1 $\dagger$	82.5 $\pm$ 0.2 $\dagger$	85.7 $\pm$ 0.2	80.3 $\pm$ 0.3 $\dagger$	86.3 $\pm$ 1.5	71.2 $\pm$ 2.1
PTC_MM	<b>71.1<math>\pm</math>6.2</b>	61.2 $\pm$ 1.1	67.9 $\pm$ 1.4	64.1 $\pm$ 1.4	62.3 $\pm$ 1.5	67.2 $\pm$ 1.6	68.0 $\pm$ 0.6 $\dagger$	67.1 $\pm$ 0.5	69.1 $\pm$ 5.0	65.9 $\pm$ 1.2
PTC_MR	64.8 $\pm$ 4.5	59.9 $\pm$ 1.7	62.5 $\pm$ 1.6	60.8 $\pm$ 1.4	59.4 $\pm$ 0.7	61.3 $\pm$ 0.9	62.5 $\pm$ 1.2	62.0 $\pm$ 1.7	<b>66.3<math>\pm</math>1.2</b>	58.3 $\pm$ 1.0
PTC_FM	<b>67.6<math>\pm</math>5.5</b>	59.4 $\pm$ 0.9	63.9 $\pm$ 1.3	61.5 $\pm$ 1.3	59.3 $\pm$ 1.3	64.4 $\pm$ 2.1	65.1 $\pm$ 1.6	64.5 $\pm$ 0.8	65.3 $\pm$ 6.2	63.9 $\pm$ 1.2
PTC_FR	<b>70.1<math>\pm</math>3.7</b>	64.3 $\pm$ 2.0	67.8 $\pm$ 1.1	65.1 $\pm$ 2.0	64.9 $\pm$ 0.9	66.2 $\pm$ 1.0	68.7 $\pm$ 1.3 $\dagger$	67.7 $\pm$ 0.3	67.3 $\pm$ 4.2	67.0 $\pm$ 1.6
ENZYMES	<b>66.7<math>\pm</math>4.7</b>	57.9 $\pm$ 5.4	60.4 $\pm$ 0.8	44.5 $\pm$ 1.6	28.2 $\pm$ 0.4	52.2 $\pm$ 1.3	57.1 $\pm$ 0.6	53.4 $\pm$ 0.9	59.1 $\pm$ 0.8	32.6 $\pm$ 1.4
PROTEINS	<b>76.6<math>\pm</math>3.4</b>	76.1 $\pm$ 2.0	75.8 $\pm$ 0.6	72.8 $\pm$ 0.7	74.2 $\pm$ 0.6	75.5 $\pm$ 0.3	75.5 $\pm$ 0.5 $\dagger$	75.7 $\pm$ 0.5	74.3 $\pm$ 0.6	75.6 $\pm$ 4.2
DD	80.3 $\pm$ 3.3	N/A	<b>81.6<math>\pm</math>0.3<math>\dagger</math></b>	78.8 $\pm$ 0.2 $\dagger$	75.6 $\pm$ 0.6 $\dagger$	79.8 $\pm$ 0.4 $\dagger$	78.6 $\pm$ 0.4	73.6 $\pm$ 0.4	79.7 $\pm$ 0.5 $\dagger$	77.0 $\pm$ 0.6
FIRSTMM_DB	<b>76.3<math>\pm</math>1.8</b>	N/A	64.8 $\pm$ 3.2	75.6 $\pm$ 0.6 $\dagger$	49.4 $\pm$ 2.9	67.0 $\pm$ 4.7	74.3 $\pm$ 2.7	73.3 $\pm$ 2.9	43.8 $\pm$ 5.7	62.8 $\pm$ 3.8
Cuneiform	78.8 $\pm$ 1.3	N/A	73.3 $\pm$ 1.1	N/A	N/A	73.4 $\pm$ 0.9	<b>81.2<math>\pm</math>1.5</b>	72.7 $\pm$ 1.0	74.4 $\pm$ 1.7	74.4 $\pm$ 1.4

TABLE III: Comparison of classification accuracy (mean  $\pm$  standard deviation) of MPG to other graph-embedding-based graph kernels on the benchmark datasets.

Dataset	MPG	DeepWalk	node2vec	LINE	GraRep	NetMF	struc2vec
KKI	<b>55.4<math>\pm</math>5.2</b>	50.7 $\pm$ 9.0	51.8 $\pm$ 10.7	50.6 $\pm$ 8.5	52.1 $\pm$ 11.2	51.8 $\pm$ 10.7	52.9 $\pm$ 8.9
MUTAG	<b>89.9<math>\pm</math>5.0</b>	83.0 $\pm$ 7.1	82.5 $\pm$ 9.5	82.5 $\pm$ 6.6	87.2 $\pm$ 6.4	80.3 $\pm$ 6.0	82.5 $\pm$ 7.8
BZR_MD	70.6 $\pm$ 5.3	63.1 $\pm$ 7.8	65.0 $\pm$ 9.8	68.0 $\pm$ 6.5	65.7 $\pm$ 9.1	<b>71.9<math>\pm</math>8.4</b>	65.7 $\pm$ 6.9
DHFR_MD	<b>73.5<math>\pm</math>5.2</b>	67.7 $\pm$ 1.6	67.9 $\pm$ 1.1	67.9 $\pm$ 1.1	65.7 $\pm$ 2.6	67.4 $\pm$ 2.0	67.7 $\pm$ 1.4
NCI1	<b>86.5<math>\pm</math>0.9</b>	71.6 $\pm$ 1.8	70.0 $\pm$ 2.0	68.2 $\pm$ 2.3	76.6 $\pm$ 1.3	70.3 $\pm$ 2.2	67.8 $\pm$ 2.5
NCI109	<b>86.7<math>\pm</math>1.6</b>	71.6 $\pm$ 2.6	69.4 $\pm$ 2.1	66.5 $\pm$ 1.1	76.4 $\pm$ 2.0	69.8 $\pm$ 2.3	68.1 $\pm$ 1.3
PTC_MM	<b>71.1<math>\pm</math>6.2</b>	64.6 $\pm$ 5.0	62.2 $\pm$ 3.1	66.4 $\pm$ 5.2	65.8 $\pm$ 6.5	65.5 $\pm$ 5.4	63.4 $\pm$ 5.5
PTC_MR	<b>64.8<math>\pm</math>4.5</b>	57.3 $\pm$ 6.1	61.0 $\pm$ 6.5	57.9 $\pm$ 5.7	56.1 $\pm$ 8.2	57.0 $\pm$ 9.1	55.2 $\pm$ 6.5
PTC_FM	<b>67.6<math>\pm</math>5.5</b>	63.0 $\pm$ 3.5	62.8 $\pm$ 1.8	64.5 $\pm$ 2.7	60.00 $\pm$ 4.5	64.2 $\pm$ 2.7	63.3 $\pm$ 3.5
PTC_FR	<b>70.1<math>\pm</math>3.7</b>	66.7 $\pm$ 4.3	68.1 $\pm$ 2.4	68.1 $\pm$ 3.3	66.7 $\pm$ 4.1	68.1 $\pm$ 3.3	66.7 $\pm$ 2.9
ENZYMES	<b>66.7<math>\pm</math>4.7</b>	48.0 $\pm$ 5.8	46.7 $\pm$ 7.6	31.7 $\pm$ 4.7	46.3 $\pm$ 6.9	36.5 $\pm$ 4.9	32.7 $\pm$ 3.6
PROTEINS	<b>76.6<math>\pm</math>3.4</b>	75.8 $\pm$ 4.4	74.7 $\pm$ 4.0	74.5 $\pm$ 3.1	73.6 $\pm$ 4.1	75.8 $\pm$ 3.8	73.9 $\pm$ 3.3
DD	<b>80.3<math>\pm</math>3.3</b>	77.8 $\pm$ 2.2	74.3 $\pm$ 3.3	78.7 $\pm$ 2.8	76.8 $\pm$ 2.7	77.4 $\pm$ 1.6	76.2 $\pm$ 2.3
FIRSTMM_DB	<b>76.3<math>\pm</math>1.8</b>	37.5 $\pm$ 3.5	39.0 $\pm$ 4.4	37.3 $\pm$ 6.3	23.0 $\pm$ 4.0	36.0 $\pm$ 2.9	39.8 $\pm$ 3.8
Cuneiform	78.8 $\pm$ 1.3	73.7 $\pm$ 1.6	79.5 $\pm$ 1.5	66.8 $\pm$ 3.1	73.3 $\pm$ 1.3	79.9 $\pm$ 1.1	<b>81.2<math>\pm</math>1.7</b>

walks. This can be simply achieved by performing random walks on the direct product graph of two input graphs. Gärtner et al. [2] introduce two closed-form solutions for random walk graph kernels, i.e., the geometric kernel and the exponential kernel. The former kernel uses the personalized PageRank diffusion [55] to aggregate every power of the adjacency matrix of the direct product graph and the latter kernel uses the heat kernel diffusion [56]. RetGK [4] assigns each node an  $S$ -dimensional feature called Return Probability Feature (RPF) that is generated by a random walk starting from a node and ending in this node with different hop length. Then, the return probabilities features and the discrete or continuous features are embedded separately into the Hilbert space where the corresponding graph kernels are computed. Borgwardt et al. [5] propose the shortest-path graph kernel (SP) that is based on the shortest paths between two nodes in graphs. SP counts the number of pairs of matching shortest paths that have the same source and sink labels and the same length in two graphs. Tree++ [6] is proposed for the problem of comparing graphs at multiple different scales. It counts the number of occurrences of path-patterns in graphs. It belongs to the R-convolution

kernels without considering the distributions of the individual substructures in graphs.

The graphlet kernel (GK) [7] decomposes a graph into small subgraph patterns having  $k$  nodes, where  $k \in \{3, 4, 5\}$ . The subgraph patterns are called graphlets [57]. Exhaustive enumeration of all graphlets are prohibitively expensive ( $\mathcal{O}(|V|^k)$ ). Thus, Shervashidze et al. [7] propose to accelerate the computation by using the method of random sampling, which is motivated by the idea that the more sufficient number of random samples is drawn, the closer the empirical distribution to the actual distribution of graphlets in a graph. Costa et al. [8] propose a novel graph kernel called the Neighborhood Subgraph Pairwise Distance Kernel (NSPDK) to decompose a graph into all pairs of neighborhood subgraphs of small radius at increasing distances. MLG [10] is developed for capturing graph structures at a range of different scales, by building a hierarchy of nested subgraphs.

Weisfeiler-Lehman subtree kernel (WL) [13], [14] is based on the Weisfeiler-Lehman test of graph isomorphism [21], which belongs to the family of color refinement algorithms that iteratively update node colors (labels) until reaching the

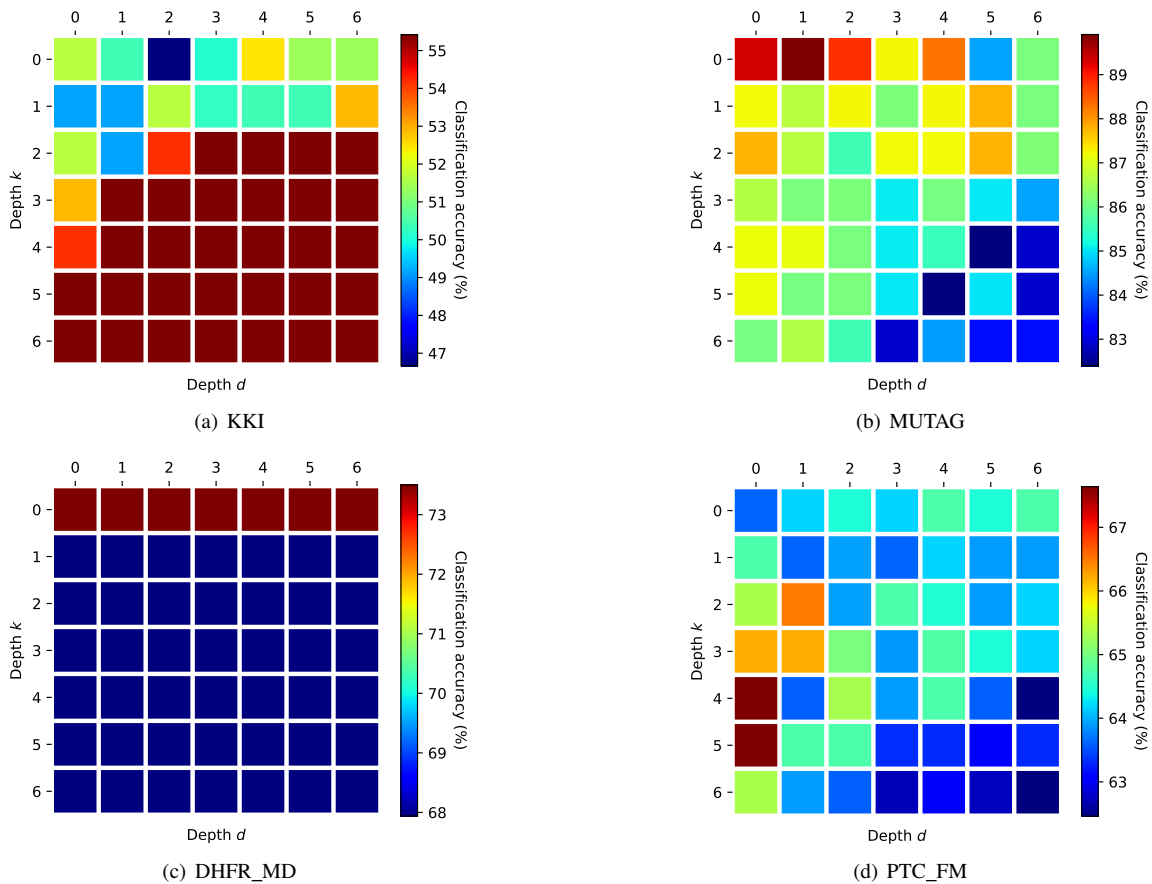


Fig. 7: Parameter sensitivity of MPG.  $d$  represents the depth of the truncated BFS tree rooted at each node and used for the extraction of path-patterns.  $k$  represents the depth of the truncated BFS tree rooted at each node and used for the construction of super paths (capturing the graph structure at multiple different scales). Each entry in the heatmap is the mean classification accuracy over the 10-fold.

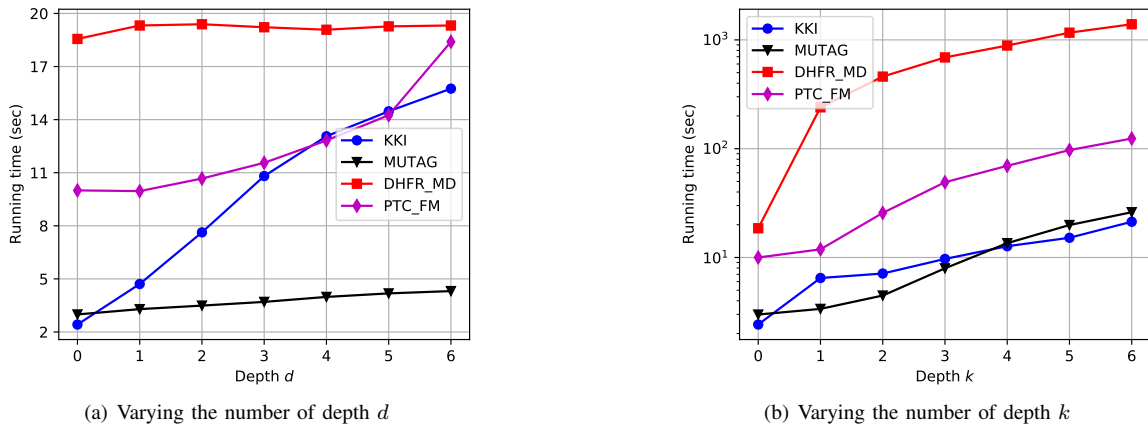


Fig. 8: The running time to compute the kernel matrix of MPG on the four datasets.

fixed number of iterations, or the node label sets of two graphs are different. WWL [16] extends WL to graphs with continuous attributes by considering each graph as a set of node embeddings and using the Wasserstein distance to com-

pute the similarity between the two sets of node embeddings. Each node has two kinds of features, one of which is the embedding generated by WL and the other of which is continuous attributes. The continuous attributes of each node are

propagated to its neighboring nodes by an average aggregation operator, which is similar to the layer-wise propagation rule of Graph Convolutional Networks (GCN) [58]. Our model MPG also uses the Wasserstein distance to compute the similarity between the node embeddings of two graphs.

There are also some works that do not belong to the above three categories. DGK utilizes word2vec [33] to learn latent representations for substructures. The similarity matrix between substructures is computed and integrated into the kernel matrix. OA [59] develops base kernels that generate graph hierarchies, from which the optimal assignment kernels are computed. The optimal assignment kernels provide a more valid notion of graph similarity, which are integrated into the WL to improve its performance. Nikolentzos et al. [17] use the eigenvectors of the graph adjacency matrices as graph embeddings and propose two graph kernels to compute the similarity between two graph embeddings. The first graph kernel uses the Earth Mover’s Distance [18] to compute the distance between two graph embeddings; and the second one uses the Pyramid Match kernel [19], [20] to find an approximate correspondence between two graph embeddings. FWL [60] is based on a filtration kernel that compares Weisfeiler-Lehman subtree feature occurrence distributions (filtration histograms) over sequences of graph resolutions. FWL’s expressiveness is more powerful than the ordinary WL. Graph Neural Tangent Kernel (GNTK) [34] is inspired by the connections between over-parameterized neural networks and kernel methods [35], [61]. It inherits both the advantages of GNN and graph kernels, i.e., extracting powerful features from graphs as GNN and being easy to train and analyze as graph kernels. It is equivalent to infinitely wide GNN trained by gradient descent.

## B. Graph Embeddings

Recently, many researchers focus on graph embedding (representation) learning, which can date back to earlier works, such as Laplacian Eigenmaps [62], multi-dimensional scaling (MDS) [63], IsoMap [64] and LPP [65]. All of these methods first construct an affinity matrix from data and then eigendecompose it. The eigenvectors are used as data embeddings, which preserve the local manifold structure in data. The time complexity of eigendecomposition is cubic with respect to the number of data points, which restricts their applications on large graphs. Now researchers transfer their attention to apply other techniques such as random walks, language model (Skip-gram [33], [37]), matrix factorization, and deep neural networks on graph embedding. For an overview of this field, we refer to literature [66]–[69].

DeepWalk [36] learns latent representations of nodes in a graph by using truncated random walks and Skip-gram. The sequences of nodes generated by truncated random walks are treated as natural language sentences. TADW [70] proves that DeepWalk is equivalent to matrix factorization. Thus, all the methods we discuss here can be categorized as matrix-factorization-based. node2vec [38] extends DeepWalk by designing a biased random walk procedure, which explores the search of neighborhood by smoothly interpolating between

two sampling strategies: breath-first sampling and depth-first sampling. GraRep [40] captures different  $k$ -step relational information among nodes by operating on different global transition matrices. It adopts matrix factorization methods to factorize each  $k$  order of the positive log probability matrix. LINE [39] considers both the first- and second-order proximity between nodes for graph embedding. NetMF [41] analyzes the Skip-gram-based graph embedding methods DeepWalk, node2vec, and LINE and proves that all of them with negative sampling can be viewed as matrix factorization. NetMF proposes to factorize the DeepWalk matrix for graph embedding. Huang et al. [71] introduce a unified view of random-walk based graph embedding and factorize the autocovariance matrix [72], [73] for graph embedding.

HOPE [74] is an embedding method for directed graphs, aiming at preserving the asymmetric transitivity, which depicts the correlation among directed edges. M-NMF [75] jointly optimizes NMF-based representation model and modularity-based community detection model to let node representations preserve both microscopic and community structures. struc2vec [42] learns latent representations for the structural identity of nodes. Nodes that have similar structural identity are closely embedded. It measures structural similarities between nodes at different scales by constructing a multilayer graph. GEMPE [76] proposes an objective function called Predictive Entropy (PE) for graph embedding. PE transfers the Euclidean distance between two nodes in the embedding space to the probability of existence of an edge between them. PINE [77] can adaptively learn an arbitrary embedding function from node neighborhood via partial permutation invariant set function. It is applicable to learn node embeddings for both homogeneous and heterogeneous graphs.

As for graph embeddings using deep neural networks, SDNE [78] incorporates the first- and second-order proximity into the objective function of the deep autoencoder. The learned non-linear latent space preserves both the local and global graph structure. DNGR [79] introduces a random surfing model to acquire graph structure information and generate a probabilistic co-occurrence matrix, based on which the Positive Pointwise Mutual Information (PPMI) matrix is computed. Then, the projection of PPMI matrix is learned by a stacked denoising autoencoder. DVNE [80] proposes a deep variational network embedding in Wasserstein space to tackle the uncertainties of the formation and evolution of real-world graphs. For each node, DVNE learns a Gaussian distribution in the Wasserstein space as its representation. DRNE [81] learns graph embeddings with regular equivalence, which is a relaxation of structural equivalence. The representation of each node is learned by a layer normalized LSTM, which recursively aggregates the neighborhood representations. NetRA [82] learns graph embeddings with adversarially regularized autoencoders, which jointly consider both locality-preserving and global reconstruction constraints. GraphSAGE [83] is developed for the inductive graph embedding. It learns a function to generate embedding for each node by sampling and aggregating features from its local neighborhood. CensNet [84] is proposed

for representation learning on graphs with both node and edge features. It transforms the original graph to line graph whose nodes represent edges in the original graph. Two graph convolutions are developed for feature propagation on each graph.

## VI. CONCLUSION

In this paper, we have proposed a novel multi-scale graph kernel called MPG to deal with the two challenges of the R-convolution graph kernels, i.e., they cannot compare graphs at multiple different scales and do not consider the distributions of substructures. To mitigate the first challenge, we propose the path-pattern node feature map, whose element represents the number of occurrences of each path-pattern around a node. Since the path-pattern node feature map cannot compare graphs at multiple different scales, we incorporate into it the multiple different scales of the graph structure, which are captured by the truncated BFS trees of different depth rooted at each node. To mitigate the second challenge, we adopt the Wasserstein distance to compute the similarity between the multi-scale path-pattern node feature maps of two graphs. Experimental results show that MPG outperforms the competing methods from both the fields of graph kernels and graph embeddings. Since the Wasserstein distance has a high time complexity, we would like to develop an efficient distance measure to compute the similarity between the embeddings of two graphs in our future work.

## REFERENCES

- [1] D. Haussler, "Convolution kernels on discrete structures," Technical report, Department of Computer Science, University of California at Santa Cruz, Tech. Rep., 1999.
- [2] T. Gärtner, P. Flach, and S. Wrobel, "On graph kernels: Hardness results and efficient alternatives," in *Learning theory and kernel machines*. Springer, 2003, pp. 129–143.
- [3] S. V. N. Vishwanathan, N. N. Schraudolph, R. Kondor, and K. M. Borgwardt, "Graph kernels," *Journal of Machine Learning Research*, vol. 11, no. Apr, pp. 1201–1242, 2010.
- [4] Z. Zhang, M. Wang, Y. Xiang, Y. Huang, and A. Nehorai, "Retgk: Graph kernels based on return probabilities of random walks," in *NIPS*, 2018, pp. 3964–3974.
- [5] K. M. Borgwardt and H.-P. Kriegel, "Shortest-path kernels on graphs," in *International Conference on Data Mining*. IEEE, 2005, pp. 8–pp.
- [6] W. Ye, Z. Wang, R. Redberg, and A. Singh, "Tree++: Truncated tree based graph kernels," *IEEE Transactions on Knowledge and Data Engineering*, 2019.
- [7] N. Shervashidze, S. Vishwanathan, T. Petri, K. Mehlhorn, and K. Borgwardt, "Efficient graphlet kernels for large graph comparison," in *Artificial Intelligence and Statistics*, 2009, pp. 488–495.
- [8] F. Costa and K. D. Grave, "Fast neighborhood subgraph pairwise distance kernel," in *ICML*. Omnipress, 2010, pp. 255–262.
- [9] T. Horváth, T. Gärtner, and S. Wrobel, "Cyclic pattern kernels for predictive graph mining," in *SIGKDD*. ACM, 2004, pp. 158–167.
- [10] R. Kondor and H. Pan, "The multiscale laplacian graph kernel," in *NIPS*, 2016, pp. 2990–2998.
- [11] J. Ramon and T. Gärtner, "Expressivity versus efficiency of graph kernels," in *Proceedings of the first international workshop on mining graphs, trees and sequences*, 2003, pp. 65–74.
- [12] P. Mahé and J.-P. Vert, "Graph kernels based on tree patterns for molecules," *Machine learning*, vol. 75, no. 1, pp. 3–35, 2009.
- [13] N. Shervashidze and K. M. Borgwardt, "Fast subtree kernels on graphs," in *Advances in neural information processing systems*, 2009, pp. 1660–1668.
- [14] N. Shervashidze, P. Schweitzer, E. J. v. Leeuwen, K. Mehlhorn, and K. M. Borgwardt, "Weisfeiler-lehman graph kernels," *Journal of Machine Learning Research*, vol. 12, no. Sep, pp. 2539–2561, 2011.
- [15] G. Da San Martino, N. Navarin, and A. Sperduti, "A tree-based kernel for graphs," in *Proceedings of the 2012 SIAM International Conference on Data Mining*. SIAM, 2012, pp. 975–986.
- [16] M. Togninalli, E. Ghisu, F. Llinares-López, B. A. Rieck, and K. Borgwardt, "Wasserstein weisfeiler-lehman graph kernels," *Advances in Neural Information Processing Systems* 32, vol. 9, pp. 6407–6417, 2020.
- [17] G. Nikolentzos, P. Meladianos, and M. Vazirgiannis, "Matching node embeddings for graph similarity," in *Thirty-first AAAI conference on artificial intelligence*, 2017.
- [18] Y. Rubner, C. Tomasi, and L. J. Guibas, "The earth mover's distance as a metric for image retrieval," *International journal of computer vision*, vol. 40, no. 2, pp. 99–121, 2000.
- [19] S. Lazebnik, C. Schmid, and J. Ponce, "Beyond bags of features: Spatial pyramid matching for recognizing natural scene categories," in *2006 IEEE computer society conference on computer vision and pattern recognition (CVPR'06)*, vol. 2. IEEE, 2006, pp. 2169–2178.
- [20] K. Grauman and T. Darrell, "The pyramid match kernel: Efficient learning with sets of features," *Journal of Machine Learning Research*, vol. 8, no. 4, 2007.
- [21] A. Leman and B. Weisfeiler, "A reduction of a graph to a canonical form and an algebra arising during this reduction," *Nauchno-Technicheskaya Informatsiya*, vol. 2, no. 9, pp. 12–16, 1968.
- [22] R. Kondor and T. Jebara, "A kernel between sets of vectors," in *Proceedings of the 20th international conference on machine learning (ICML-03)*, 2003, pp. 361–368.
- [23] F. Harary, "Graph theory addison-wesley reading ma usa," 1969.
- [24] C. Villani, *Optimal transport: old and new*. Springer, 2009, vol. 338.
- [25] A. Figalli and C. Villani, "Optimal transport and curvature," in *Nonlinear PDE's and Applications*. Springer, 2011, pp. 171–217.
- [26] B. Haasdonk and C. Bahlmann, "Learning with distance substitution kernels," in *Joint pattern recognition symposium*. Springer, 2004, pp. 220–227.
- [27] G. Loosli, S. Canu, and C. S. Ong, "Learning svm in krein spaces," *IEEE transactions on pattern analysis and machine intelligence*, vol. 38, no. 6, pp. 1204–1216, 2015.
- [28] M. Togninalli, E. Ghisu, F. Llinares-López, B. Rieck, and K. Borgwardt, "Wasserstein weisfeiler-lehman graph kernels," *Advances in Neural Information Processing Systems*, vol. 32, 2019.
- [29] A. Gretton, K. M. Borgwardt, M. J. Rasch, B. Schölkopf, and A. Smola, "A kernel two-sample test," *The Journal of Machine Learning Research*, vol. 13, no. 1, pp. 723–773, 2012.
- [30] M. Neumann, R. Garnett, C. Bauckhage, and K. Kersting, "Propagation kernels: efficient graph kernels from propagated information," *Machine Learning*, vol. 102, no. 2, pp. 209–245, 2016.
- [31] B. Weisfeiler and A. Lehman, "A reduction of a graph to a canonical form and an algebra arising during this reduction," *Nauchno-Technicheskaya Informatsiya*, vol. 2, no. 9, pp. 12–16, 1968.
- [32] P. Yanardag and S. Vishwanathan, "Deep graph kernels," in *Proceedings of the 21th ACM SIGKDD International Conference on Knowledge Discovery and Data Mining*. ACM, 2015, pp. 1365–1374.
- [33] T. Mikolov, K. Chen, G. Corrado, and J. Dean, "Efficient estimation of word representations in vector space," *arXiv preprint arXiv:1301.3781*, 2013.
- [34] S. S. Du, K. Hou, B. Póczos, R. Salakhutdinov, R. Wang, and K. Xu, "Graph neural tangent kernel: Fusing graph neural networks with graph kernels," in *Advances in Neural Information Processing Systems*, 2019.
- [35] A. Jacot, F. Gabriel, and C. Hongler, "Neural tangent kernel: Convergence and generalization in neural networks," in *Advances in neural information processing systems*, 2018, pp. 8571–8580.
- [36] B. Perozzi, R. Al-Rfou, and S. Skiena, "Deepwalk: Online learning of social representations," in *Proceedings of the 20th ACM SIGKDD international conference on Knowledge discovery and data mining*. ACM, 2014, pp. 701–710.
- [37] T. Mikolov, I. Sutskever, K. Chen, G. S. Corrado, and J. Dean, "Distributed representations of words and phrases and their compositionality," in *Advances in neural information processing systems*, 2013, pp. 3111–3119.
- [38] A. Grover and J. Leskovec, "node2vec: Scalable feature learning for networks," in *Proceedings of the 22nd ACM SIGKDD international conference on Knowledge discovery and data mining*. ACM, 2016, pp. 855–864.

- [39] J. Tang, M. Qu, M. Wang, M. Zhang, J. Yan, and Q. Mei, "Line: Large-scale information network embedding," in *Proceedings of the 24th International Conference on World Wide Web*. International World Wide Web Conferences Steering Committee, 2015, pp. 1067–1077.
- [40] S. Cao, W. Lu, and Q. Xu, "Grarep: Learning graph representations with global structural information," in *Proceedings of the 24th ACM International Conference on Information and Knowledge Management*. ACM, 2015, pp. 891–900.
- [41] J. Qiu, Y. Dong, H. Ma, J. Li, K. Wang, and J. Tang, "Network embedding as matrix factorization: Unifying deepwalk, line, pte, and node2vec," in *Proceedings of the eleventh ACM international conference on web search and data mining*, 2018, pp. 459–467.
- [42] L. F. Ribeiro, P. H. Saverese, and D. R. Figueiredo, "struc2vec: Learning node representations from structural identity," in *Proceedings of the 23rd ACM SIGKDD International Conference on Knowledge Discovery and Data Mining*. ACM, 2017, pp. 385–394.
- [43] G. Siglidis, G. Nikolentzos, S. Limnios, C. Giatsidis, K. Skianis, and M. Vazirgiannis, "Grakel: A graph kernel library in python," *arXiv preprint arXiv:1806.02193*, 2018.
- [44] C.-C. Chang and C.-J. Lin, "Libsvm: a library for support vector machines," *TIST*, vol. 2, no. 3, p. 27, 2011.
- [45] K. Kersting, N. M. Kriege, C. Morris, P. Mutzel, and M. Neumann, "Benchmark data sets for graph kernels," 2016. [Online]. Available: <http://graphkernels.cs.tu-dortmund.de>
- [46] S. Pan, J. Wu, X. Zhu, G. Long, and C. Zhang, "Task sensitive feature exploration and learning for multitask graph classification," *IEEE transactions on cybernetics*, vol. 47, no. 3, pp. 744–758, 2017.
- [47] A. K. Debnath, R. L. Lopez de Compadre, G. Debnath, A. J. Shusterman, and C. Hansch, "Structure-activity relationship of mutagenic aromatic and heteroaromatic nitro compounds. correlation with molecular orbital energies and hydrophobicity," *Journal of medicinal chemistry*, vol. 34, no. 2, pp. 786–797, 1991.
- [48] J. J. Sutherland, L. A. O'Brien, and D. F. Weaver, "Spline-fitting with a genetic algorithm: A method for developing classification structure-activity relationships," *Journal of chemical information and computer sciences*, vol. 43, no. 6, pp. 1906–1915, 2003.
- [49] N. Wale, I. A. Watson, and G. Karypis, "Comparison of descriptor spaces for chemical compound retrieval and classification," *Knowledge and Information Systems*, vol. 14, no. 3, pp. 347–375, 2008.
- [50] N. Kriege and P. Mutzel, "Subgraph matching kernels for attributed graphs," *arXiv preprint arXiv:1206.6483*, 2012.
- [51] K. M. Borgwardt, C. S. Ong, S. Schönauer, S. Vishwanathan, A. J. Smola, and H.-P. Kriegel, "Protein function prediction via graph kernels," *Bioinformatics*, vol. 21, no. suppl\_1, pp. i47–i56, 2005.
- [52] P. D. Dobson and A. J. Doig, "Distinguishing enzyme structures from non-enzymes without alignments," *Journal of molecular biology*, vol. 330, no. 4, pp. 771–783, 2003.
- [53] M. Neumann, P. Moreno, L. Antanas, R. Garnett, and K. Kersting, "Graph kernels for object category prediction in task-dependent robot grasping," in *Online proceedings of the eleventh workshop on mining and learning with graphs*, 2013, pp. 0–6.
- [54] N. M. Kriege, M. Fey, D. Fisseler, P. Mutzel, and F. Weichert, "Recognizing cuneiform signs using graph based methods," in *International Workshop on Cost-Sensitive Learning*. PMLR, 2018, pp. 31–44.
- [55] R. Andersen, F. Chung, and K. Lang, "Local graph partitioning using pagerank vectors," in *2006 47th Annual IEEE Symposium on Foundations of Computer Science (FOCS'06)*. IEEE, 2006, pp. 475–486.
- [56] F. Chung, "The heat kernel as the pagerank of a graph," *Proceedings of the National Academy of Sciences*, vol. 104, no. 50, pp. 19 735–19 740, 2007.
- [57] N. Pržulj, D. G. Corneil, and I. Jurisica, "Modeling interactome: scale-free or geometric?" *Bioinformatics*, vol. 20, no. 18, pp. 3508–3515, 2004.
- [58] T. N. Kipf and M. Welling, "Semi-supervised classification with graph convolutional networks," *International Conference on Learning Representations (ICLR)*, 2016.
- [59] N. M. Kriege, P.-L. Giscard, and R. Wilson, "On valid optimal assignment kernels and applications to graph classification," in *Advances in Neural Information Processing Systems*, 2016, pp. 1623–1631.
- [60] T. H. Schulz, P. Welke, and S. Wrobel, "Graph filtration kernels," in *Proceedings of the AAAI Conference on Artificial Intelligence*, 2022.
- [61] S. Arora, S. S. Du, W. Hu, Z. Li, R. Salakhutdinov, and R. Wang, "On exact computation with an infinitely wide neural net," *arXiv preprint arXiv:1904.11955*, 2019.
- [62] M. Belkin and P. Niyogi, "Laplacian eigenmaps and spectral techniques for embedding and clustering," in *Advances in neural information processing systems*, 2002, pp. 585–591.
- [63] M. L. Davison, "Multidimensional scaling," 1991.
- [64] J. B. Tenenbaum, V. De Silva, and J. C. Langford, "A global geometric framework for nonlinear dimensionality reduction," *science*, vol. 290, no. 5500, pp. 2319–2323, 2000.
- [65] X. He and P. Niyogi, "Locality preserving projections," in *Advances in neural information processing systems*, 2004, pp. 153–160.
- [66] H. Cai, V. W. Zheng, and K. C.-C. Chang, "A comprehensive survey of graph embedding: Problems, techniques, and applications," *IEEE Transactions on Knowledge and Data Engineering*, vol. 30, no. 9, pp. 1616–1637, 2018.
- [67] P. Cui, X. Wang, J. Pei, and W. Zhu, "A survey on network embedding," *IEEE transactions on knowledge and data engineering*, vol. 31, no. 5, pp. 833–852, 2018.
- [68] W. L. Hamilton, R. Ying, and J. Leskovec, "Representation learning on graphs: Methods and applications," *arXiv preprint arXiv:1709.05584*, 2017.
- [69] P. Goyal and E. Ferrara, "Graph embedding techniques, applications, and performance: A survey," *Knowledge-Based Systems*, vol. 151, pp. 78–94, 2018.
- [70] C. Yang, Z. Liu, D. Zhao, M. Sun, and E. Y. Chang, "Network representation learning with rich text information," in *IJCAI*, 2015, pp. 2111–2117.
- [71] Z. Huang, A. Silva, and A. Singh, "A broader picture of random-walk based graph embedding," in *Proceedings of the 27th ACM SIGKDD Conference on Knowledge Discovery & Data Mining*, 2021, pp. 685–695.
- [72] J.-C. Delvenne, M. T. Schaub, S. N. Yaliraki, and M. Barahona, "The stability of a graph partition: A dynamics-based framework for community detection," in *Dynamics On and Of Complex Networks, Volume 2*. Springer, 2013, pp. 221–242.
- [73] J.-C. Delvenne, S. N. Yaliraki, and M. Barahona, "Stability of graph communities across time scales," *Proceedings of the national academy of sciences*, vol. 107, no. 29, pp. 12 755–12 760, 2010.
- [74] M. Ou, P. Cui, J. Pei, Z. Zhang, and W. Zhu, "Asymmetric transitivity preserving graph embedding," in *Proceedings of the 22nd ACM SIGKDD international conference on Knowledge discovery and data mining*. ACM, 2016, pp. 1105–1114.
- [75] X. Wang, P. Cui, J. Wang, J. Pei, W. Zhu, and S. Yang, "Community preserving network embedding," in *AAAI*, 2017, pp. 203–209.
- [76] C. Plant, S. Biedermann, and C. Böhm, "Data compression as a comprehensive framework for graph drawing and representation learning," in *Proceedings of the 26th ACM SIGKDD International Conference on Knowledge Discovery & Data Mining*, 2020, pp. 1212–1222.
- [77] S. Gui, X. Zhang, P. Zhong, S. Qiu, M. Wu, J. Ye, Z. Wang, and J. Liu, "Pine: Universal deep embedding for graph nodes via partial permutation invariant set functions," *IEEE Transactions on Pattern Analysis and Machine Intelligence*, vol. 44, no. 2, pp. 770–782, 2021.
- [78] D. Wang, P. Cui, and W. Zhu, "Structural deep network embedding," in *Proceedings of the 22nd ACM SIGKDD international conference on Knowledge discovery and data mining*. ACM, 2016, pp. 1225–1234.
- [79] S. Cao, W. Lu, and Q. Xu, "Deep neural networks for learning graph representations," in *AAAI*, 2016, pp. 1145–1152.
- [80] D. Zhu, P. Cui, D. Wang, and W. Zhu, "Deep variational network embedding in wasserstein space," in *Proceedings of the 24th ACM SIGKDD International Conference on Knowledge Discovery & Data Mining*. ACM, 2018, pp. 2827–2836.
- [81] K. Tu, P. Cui, X. Wang, P. S. Yu, and W. Zhu, "Deep recursive network embedding with regular equivalence," in *Proceedings of the 24th ACM SIGKDD International Conference on Knowledge Discovery and Data Mining*. ACM, 2018, pp. 2357–2366.
- [82] W. Yu, C. Zheng, W. Cheng, C. C. Aggarwal, D. Song, B. Zong, H. Chen, and W. Wang, "Learning deep network representations with adversarially regularized autoencoders," in *Proceedings of the 24th ACM SIGKDD International Conference on Knowledge Discovery & Data Mining*. ACM, 2018, pp. 2663–2671.
- [83] W. Hamilton, Z. Ying, and J. Leskovec, "Inductive representation learning on large graphs," in *Advances in Neural Information Processing Systems*, 2017, pp. 1024–1034.
- [84] X. Jiang, R. Zhu, S. Li, and P. Ji, "Co-embedding of nodes and edges with graph neural networks," *IEEE Transactions on Pattern Analysis and Machine Intelligence*, 2020.